Rare Metal Materials and Engineering
Volume 51, Issue 2, February 2022
Available online at www.rmme.ac.cn

Science Press

Cite this article as: Jia Zhi, Yu Lidan, Wei Baolin, et al. High-Temperature Thermal Deformation Behavior and Microstructural Evolution of Inconel 617 Alloy[J]. Rare Metal Materials and Engineering, 2022, 51(02): 461-468.

ARTICLE

High-Temperature Thermal Deformation Behavior and Microstructural Evolution of Inconel 617 Alloy

Jia Zhi[1,2], Yu Lidan[1], Wei Baolin[1], Sun Xuan[1], Wang Yanjiang[1], Liu Dexue[1], Ding Yutian[1]

[1] School of Materials Science and Engineering, Lanzhou University of Technology, Lanzhou 730050, China; [2] State Key Laboratory of Advanced Processing and Recycling of Nonferrous Metals, Lanzhou University of Technology, Lanzhou 730050, China

Abstract: To solve the problems of processing Inconel 617 alloy at high temperatures, the hot deformation behavior of forged Inconel 617 at high temperature was studied. A Gleeble-3500 instrument was used to analyze the thermoplastic behavior in the temperature range of 900~1200 °C and strain rate range of 0.001~10 s^{-1}. The constitutive equation in this temperature and strain rate range was deduced, and the thermal processing map was obtained. The dynamic recrystallization after compression was studied by electron backscatter diffraction. The location of the instability zone was determined. Results show that under the conditions of thermal deformation, dynamic recrystallization occurs, and fine grains are obtained. The optimal temperature range for Inconel 617 thermal processing is identified as 1075~1175 °C, and this temperature range is in the stable zone for the material.

Key words: thermal compression; constitutive equation; processing diagram; recrystallization

Inconel 617 is a nickel-based solid solution strengthened superalloy with nickel, chromium, cobalt, aluminum, and molybdenum as the main elements. It displays high creep strength and good corrosion resistance. Due to the presence of chromium and aluminum in the alloy, a protective oxide layer is formed on the alloy surface, which enhances its anti-oxidation property. Inconel 617 can be used in a wide range of applications in aerospace, nuclear power, boilers, steam parts and other fields. It has good thermal processing performance similar to Inconel 625, and can be processed by cold processing with the standard production method. However, it requires intermediate annealing. Its welding performance is also very good, and compared with Inconel 625 it shows clear advantages in some performance characteristics[1-6].

Thermal deformation is a critical step for the study of nickel-based superalloys due to their high resistance to degradation and uneven content of the precipitated phase. Chen et al [7] conducted a simulation of the microstructure of the GH4698 nickel-based superalloy during thermal deformation, analyzed the relationship between the deformation parameters and microstructure evolution, and established a dynamic recrystallization kinetic model. Gao et al[8] studied the effect of the homogenization treatment on thermal deformation behavior of the GH3625 alloy. Cheng et al[9] formulated the thermal extrusion process parameters of 028-nickel-based tubing and studied the thermal deformation of this alloy in the temperature range of 950~1200 °C. Wu et al[10] studied the deformation behavior of Nimonic 80A materials in the temperature range of 800~1180 ° C, and determined the transition temperature of the dynamic recrystallization mechanism. Han et al[11] conducted an in-depth study on the thermal deformation behavior and processing diagram of the U720Li nickel-based superalloy, which is highly significant and valuable for the process formulation and theoretical simulation of the U720Li alloy. The constitutive equation is usually used to describe the relationship between flow stress and strain. For the materials undergoing a thermoplastic deformation process, the flow stress is not only related to stress, but also to the temperature, deformation rate, deformation and material structure, as specified in the constitutive equation that is used to characterize the deformation characteristics of the material

Received date: February 16, 2021
Foundation item: National Nature Science Foundation of China (51665032); Science Foundation for Distinguished Young Scholars of Gansu Province (18JR3RA134); Lanzhou University of Technology Support Plan for Excellent Young Scholars (CGZH001)
Corresponding author: Jia Zhi, Ph. D., Associate Professor, State Key Laboratory of Advanced Processing and Recycling of Nonferrous Metals, Lanzhou University of Technology, Lanzhou 730050, P. R. China, E-mail: jiazhi@lut.edu.cn

and the influence of the process parameters on the flow stress and microstructure of the material during the deformation process [12,13]. In the thermal compression process of Inconel 617, the constitutive relation proposed by Sellars[14] is used to describe the effect of the temperature and deformation rate on the rheological stress.

There are few researches on the hot deformation behavior of the Inconel 617 alloy, especially on the hot deformation behavior and microstructure evolution of forged Inconel 617 alloy. Therefore, this work focused on the experimental investigation of the behavior, especially its microstructural evolution, of the Inconel 617 alloy during the process of hot deformation. Using Inconel 617 as the research object, we performed hot compression experiments at 900, 1000, 1100, and 1200 °C and at the strain rates of 0.001, 0.01, 0.1, 1, and 10 s^{-1} using a GIeebIe-3500 simulation system. The true stress-strain curves, and the constitutive equation for Inconel 617 under the experimental conditions were obtained, the processing diagram was constructed, and the microstructure was analyzed by electron backscattered diffraction (EBSD). This work will provide theoretical guidance and practical basis for the heat treatment process of Inconel 617 in the future.

1 Experiment

Inconel 617 provided by Jinchuan Nickel Alloy Co., Ltd, was used in this work. The chemical composition of this alloy is shown in Table 1. Since the as-cast material cracks easily when compressed at high temperature, the forged material was used.

The dimensions of the samples used in the experiments are *Φ*8 mm×12 mm. A Gleeble-3500 thermal simulation instrument was used to conduct the hot compression experiments at the temperatures of 900, 1000, 1100 and 1200 °C and strain rates of 0.001, 0.01, 0.1, 1, and 10 s^{-1}. To reduce the influence of friction on the experimental results obtained during the compression process, tantalum chips were placed at both ends of each sample prior to compression. Fig. 1 shows the original microstructure and it is observed that all of the grains in the sample have essentially the same size.

After the hot compression experiment, the compressed material was cut by a cutting machine, emery of different grades was used for metallographic grinding and polishing, and then the sample was corroded by aqua regia to observe the microstructure. Finally, EBSD measurements were performed to characterize the microstructure orientation.

2 Results and Discussion

2.1 True stress-strain curve analysis

Fig. 2 shows the true stress-strain curves of the 617 alloy under different deformation temperatures and different strain

Table 1 Major chemical compositions of Inconel 617 alloy (wt%)

Cr	Mo	Al	Co	Fe	C	Si	Ti	Ni
20.8	9.12	1.28	13.1	0.8	0.07	0.11	0.22	Bal.

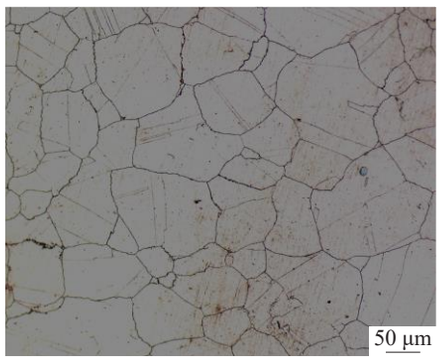

Fig.1 Original microstructure of sample

rates. The overall trend of the curve is that the flow stress rapidly increases to the peak as the degree of deformation increases, then slowly decreases, and finally tends to stabilize. The trend of this true stress-strain curve is fully consistent with the plasticity change of metal with low stacking fault energy. The evolution characteristics of flow stress during the deformation process indicate that the grains undergo dynamic recrystallization during the thermal compression process. At a given strain rate, the stress decreases with increasing the temperature, and at a given deformation temperature, it is opposite. This is mainly because deformation is a thermally activated process. As the temperature increases, the average kinetic energy of the atoms increases, and the critical shear stress for crystal grain slip decreases, resulting in a decrease in the resistance to dislocation movement and crystal slip.

Some curves exhibit sharp fluctuations that are caused by the alternation of the softening due to recrystallization and grain growth at high temperatures and the hardening caused by the re-deformation of the recrystallized grains. Before the stress reaches the peak value, the work hardening effect is dominated. As the amount of deformation continues to increase, the dislocation density continues to rise. After a certain amount of deformation, the deformation storage energy becomes the driving force in the recrystallization process, giving rise to dynamic recrystallization. The softening effect gradually plays an increasingly pronounced role until the hardening effect strength caused by deformation and softening effect strength caused by recrystallization become equal, so the flow stress tends to a stable value and the curve enters into the steady state stage.

At small strain rates, the rheological curve decreases to a stable value more rapidly after reaching the peak, while at high strain rates such as 1 and 10 s^{-1}, the rheological curve after the peak returns to a stable value relatively slowly, showing a smooth decline. Previous studies have suggested that this is due to adiabatic temperature rise. As the strain rate increases, the influence of the adiabatic temperature rise on the rheological curve will be more pronounced and non-negligible.

During thermal deformation, both deformation and temperature rise will occur in metal materials; this is known as the adiabatic temperature rise effect and is closely related to

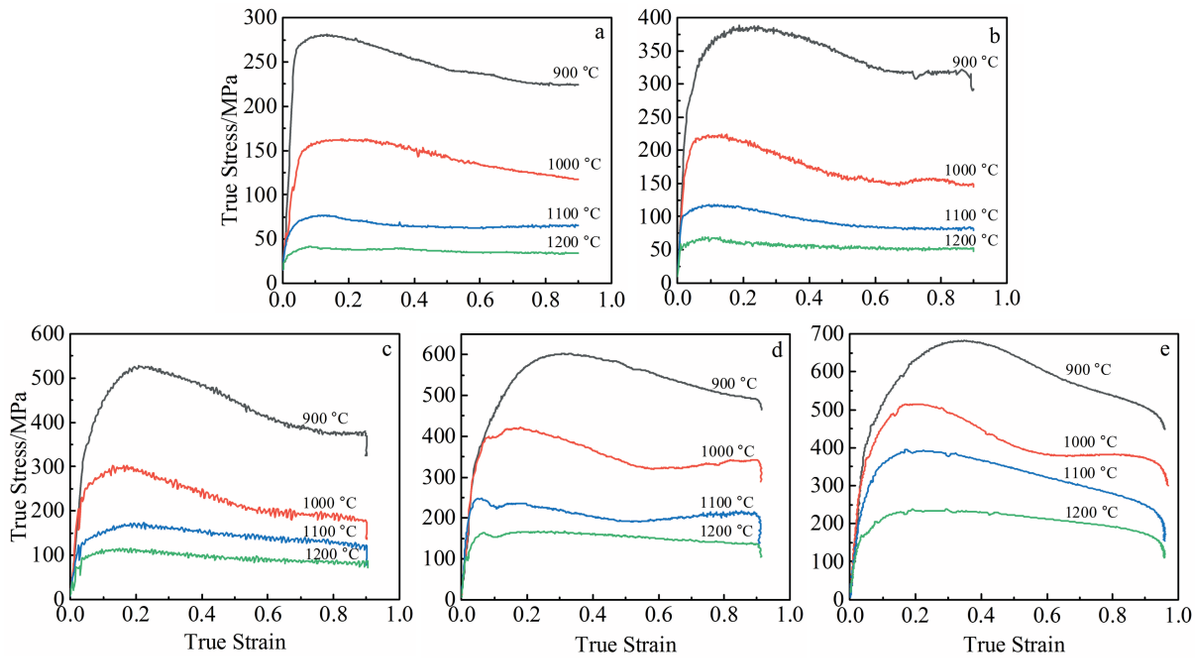

Fig.2 True stress-strain curves under different deformation temperatures and different strain rates: (a) 0.001 s^{-1}, (b) 0.01 s^{-1}, (c) 0.1 s^{-1}, (d) 1 s^{-1}, and (e) 10 s^{-1}

the strain rate. Currently, the adiabatic temperature rise effect of metal materials during the thermal compression process is generally studied using Eq.(1):

$$\Delta T = \frac{0.95\delta}{\rho C_p}\int_0^{\varepsilon}\sigma \mathrm{d}\varepsilon \tag{1}$$

$$\delta = \begin{cases} 0 & \dot{\varepsilon} \leqslant 10^{-3}\ s^{-1} \\ 0.316\lg\dot{\varepsilon} + 0.95 & 10^{-3}\ s^{-1} < \dot{\varepsilon} < 1\ s^{-1} \\ 0.95 & \dot{\varepsilon} \geqslant 1\ s^{-1} \end{cases} \tag{2}$$

where δ is the adiabatic factor that is a function of the deformation rate, as given in Eq.(2), ρ is the density, C_p is the specific heat capacity (0.662 J/g·°C), σ is the flow stress, ε is the true strain, and $\dot{\varepsilon}$ is the strain rate. As observed from Fig.3, with increasing the strain rate, the adiabatic temperature rise becomes obvious, and its influence on the material during the deformation at the strain rates of 1 and 10 s^{-1} cannot be ignored. At 900 °C, strain rates of 1 and 10 s^{-1}, and compression of 60%, the temperature rise reaches 70 °C. If the effect of the adiabatic temperature rise on the rheological curve is removed, the stress peak of the curve will increase significantly and the softening phenomenon in the later deformation will also be weakened. Therefore, it is highly important to study the rheological curves and use them to derive the properties of materials.

2.2 Constitutive equation

The constitutive equation is used to describe the relationship between the flow stress and the strain of the material during deformation. Rheological stress and strain, strain rate, and temperature are related by the constitutive equation [15]: $\sigma = f(\varepsilon,\dot{\varepsilon},T)$. In the process of high-temperature deformation, the flow stress depends mainly on the strain rate and deformation temperature, as described by the Arrhenius

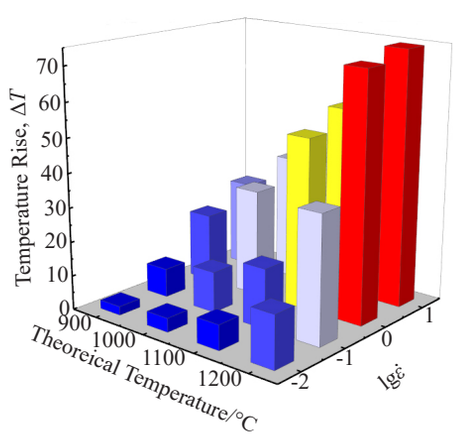

Fig.3 Adiabatic temperature rise diagram during hot compression of Inconel 617 alloy

relationship:

$$\dot{\varepsilon} = Z = A\dot{\varepsilon}\exp\left(\frac{-Q}{RT}\right) \tag{3}$$

where Z is the Zener-Hollomon parameter that relates the strain rate and the temperature to the strain-stress behavior of the material, Q is the deformation activation energy of the material that measures the degree of the high-temperature deformation, A is a constant, R is the gas constant that is equal to 8.314 J/mol, and T is the deformation temperature. The equivalent strain rate, $f(\sigma)$, for the rheological stress function according to the stress level has the following three forms, given by Eq.(4~6):

$$\dot{\varepsilon} = Z = K_1\sigma^{n_1}\exp\left(\frac{-Q}{RT}\right) \qquad \alpha\sigma<0.8 \tag{4}$$

$$\dot{\varepsilon} = Z = K_2\exp(\beta\sigma)\exp\left(\frac{-Q}{RT}\right) \qquad \alpha\sigma>1.2 \tag{5}$$

$$\dot{\varepsilon} = Z = K[\sinh(\alpha\sigma)]^n \exp\left(\frac{-Q}{RT}\right) \quad \text{For all stress} \qquad (6)$$

where K_1, K_2, and K are constants, n is the stress index, $\alpha=\beta/n$, and the optimized α value is generally between 0.01 and 0.016. Eq. (4) is the commonly used creep power function expression that is used for the modeling of the constitutive behavior of materials under high-temperature and low-stress conditions. Eq. (5) is an exponential function constitutive relation that is used to describe the constitutive behavior of materials under high-stress conditions. However, when the high temperature and strain rate are less than 1, β will change with the change of the strain rate. Eq. (6) applies to all stress values.

Taking logarithm on both sides of Eq. (4~6), the curves of $\ln\dot{\varepsilon}$ - $\ln\sigma$, $\ln\dot{\varepsilon}$ - σ, $\ln\dot{\varepsilon}$ - $\ln[\sinh(\alpha\sigma)]$ were plotted and unitary linear fitting was performed. At a constant deformation temperature, Q, R, T, and K are all constants, and taking logarithm on both sides of Eq. (4~6) gives:

$$\ln\dot{\varepsilon} = \ln K_1 + n_1 \ln\sigma - Q/RT \qquad (7)$$

$$\ln\dot{\varepsilon} = \ln K_2 + \beta\sigma - Q/RT \qquad (8)$$

$$\ln\dot{\varepsilon} = \ln K + n\ln[\sinh(\alpha\sigma)] - Q/RT \qquad (9)$$

It is observed from Eq. (7) and Eq. (8) that a linear relationship exists between $\ln\dot{\varepsilon}$ - $\ln\sigma$ and $\ln\dot{\varepsilon}$ - σ. The average value of the reciprocal slope of the line in Eq.(7) is n_1, and the reciprocal slope of the line for Eq. (8) is β. Taking the peak stress of different deformation conditions, and fitting the linear relationship between $\ln\sigma$-$\ln\dot{\varepsilon}$ and σ-$\ln\dot{\varepsilon}$, Fig.4 can be obtained. An examination of Fig.4a shows that n_1 is 7.245 451 227, and it is observed from Fig.4b that β is 0.031 169 522. Since $\alpha=\beta/n_1$, α=0.004 301 944 MPa^{-1}.

For a given temperature, partial differentiation of Eq.(9) can be used to obtain the thermal deformation activation energy Q:

$$Q = R\frac{\partial\ln\dot{\varepsilon}}{\partial\ln[\sinh(\alpha\sigma)]}\Big|_T \frac{\partial\ln[\sinh(\alpha\sigma)]}{\partial T^{-1}}\Big|_\varepsilon \qquad (10)$$

The relationship between $\ln[\sinh(\alpha\sigma)]$ - $\ln\dot{\varepsilon}$ and $\ln[\sinh(\alpha\sigma)]$-T^{-1} was obtained using the data of the peak stress under different deformation conditions, as shown in Fig.5, and linear regression was performed.

From Fig. 5a, it is obtained that n is 4.823 970 408, as described by:

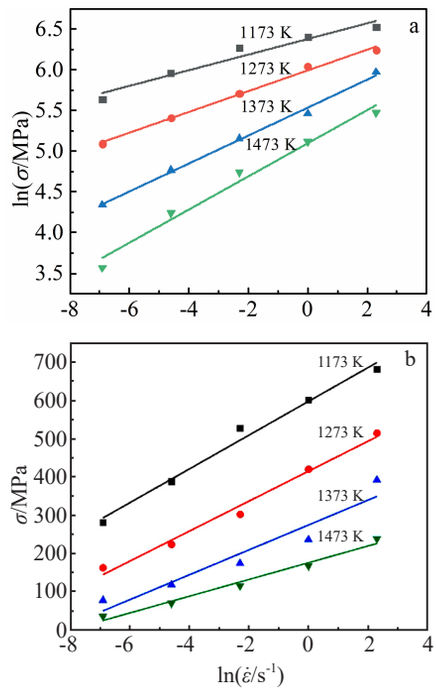

Fig.4 Relationship between the peak stress and strain rate during high-temperature compression of the Inconel 617 alloy: (a) $\ln\sigma$ - $\ln\dot{\varepsilon}$ and (b) σ - $\ln\dot{\varepsilon}$

$$\frac{\partial\ln\dot{\varepsilon}}{\partial\ln[\sinh(\alpha\sigma)]}\Big|_T = 4.823\,970\,408 = n \qquad (11)$$

Examination of the data presented in Fig.5b shows that

$$(\partial\ln[\sinh(\alpha\sigma)]/(\partial T^{-1})|_{\dot{\varepsilon}} = 12.538\,146 \qquad (12)$$

Therefore, the deformation activation energy Q can be calculated as 502.861 03 kJ/mol.

For Eq (9), it is observed that when T is fixed, The average of the reciprocal slope of line is n, and the linear intercept is $[Q/(RT)-\ln K]/n$, and n and K can be obtained, with n=4.823 970 408. Using Fig. 5a and formula $[Q/(RT)-\ln K]/n$ to obtain $\ln K$, the average value of four $\ln K$ is calculated as 42.426 326 14. That is, $\ln K$ is 42.426 326 14, so K is 2.66391×10^{18}, and the constitutive equation for the thermoplastic deformation process of Inconel 617 alloy is given by:

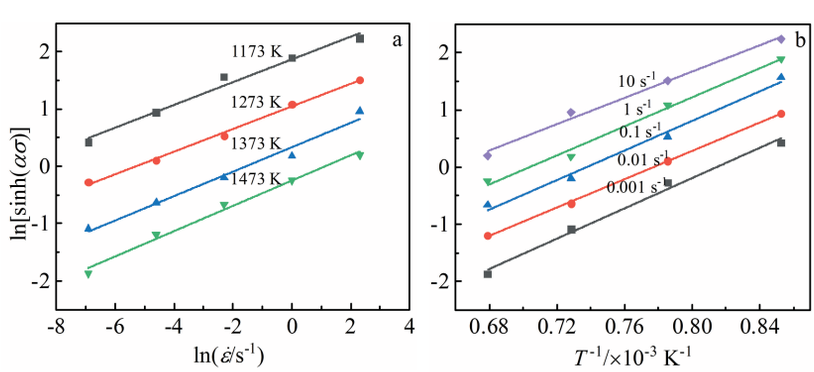

Fig.5 Relationship between $\ln[(\sinh(\alpha\sigma)]$ - $\ln\dot{\varepsilon}$ (a) and $\ln[\sinh(\alpha\sigma)]$-T^{-1} (b)

$$\dot{\varepsilon}=2.663\ 91\times10^{18}[\sinh(0.004\ 301\ 944\sigma)]^{4.823\ 970\ 408}\times\exp(-502.861\ 03/RT) \quad (13)$$

To verify the accuracy of the constitutive equation, the peak stress values calculated under different strain rates and temperatures are compared to the experimental results in Fig.6. It is observed that there is outlier data point that may be due to the friction between the material used in the experiment and the pressure head or the center of pressure head caused by misalignment. Except this data point, the data show reasonable accuracy. The maximum error between the predicted peak stress and the experimental peak stress is only 18.5%, and the average error is 5%. The predicted stress values are basically consistent with the experimental stress values. Therefore, the constitutive equation obtained in this experiment is correct.

2.3 Processing diagram of hot compression process

The processing diagram describes the degree of deformation that the metal material can achieve without being destroyed under the action of external forces in the process of plastic deformation. The working diagram provides a measure of the processing quality and metal plastic forming ability that is an important property for application[16-19]. The criterion for processing instability was established by Prasad et al[20]. According to the principle of maximum entropy generation rate proposed by Ziegler[21], the maximum principle of irreversible thermal dynamics was applied to large strain plastic deformation to obtain the material instability criterion:

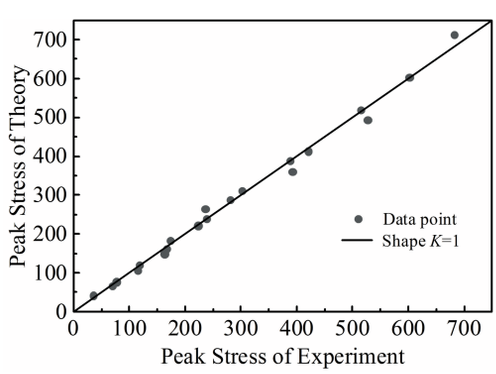

Fig.6 Comparison of the theoretical peak stress and experimental peak stress

$$\xi(\dot{\varepsilon})=\frac{\partial\ln\left(\frac{m}{m+1}\right)}{\partial\ln\dot{\varepsilon}}+m<0 \quad (14)$$

The region with the negative value represents the instability region. The physical meaning of this equation is as follows: if the system cannot generate entropy at a rate greater than the strain rate applied on the system, the system will produce rheological instability. The strain rate sensitivity index can be obtained from the stress-strain data obtained by thermal compression, and then the dissipated power can be obtained according to:

$$\eta=J/J_{max}=2m/(m+1) \quad (15)$$

The instability diagram and dissipation diagram were drawn, and then were superimposed to form the processing diagram.

Fig.7 shows the hot working diagram of Inconel 617, where the shaded region is the rheological instability zone. The working diagrams under different deformation amounts are roughly similar. For the strain rates less than 0.01 s^{-1}, the system is stable in the entire temperature range. When the strain rate is higher than 0.01 s^{-1}, high-temperature and high-rate instability zones and low-temperature instability zones are observed. With the increase in the temperature and decrease in the strain rate, the dissipation factor increases continuously, but with the increase in the strain rate, the range of variation of the dissipation factor is not large.

Analysis of the processing diagram at the strain of 0.6 shows two obvious instability regions; the first region is the buckling area in the temperature range of 900~1075 °C and the strain rate range of 0.1~10 s^{-1}. This region is located in the high-strain rate and low-temperature part of the diagram. This result is because the dynamic recrystallization is a process of thermal activation and intracrystalline energy storage at low temperature is low and not sufficient to fully carry out the dynamic recrystallization in the alloy. This leads to uneven deformation and the appearance of the rheological instability. The second instability zone is found in the high temperature and high strain rate region of the diagram in the temperature range of 1175~1200 °C and the strain rate range of 0.1~10 s^{-1}. It is because at high temperature and high strain rate, due to the short time, a large amount of heat is too late to diffuse, and the temperature of the core of the sample rises, which is more

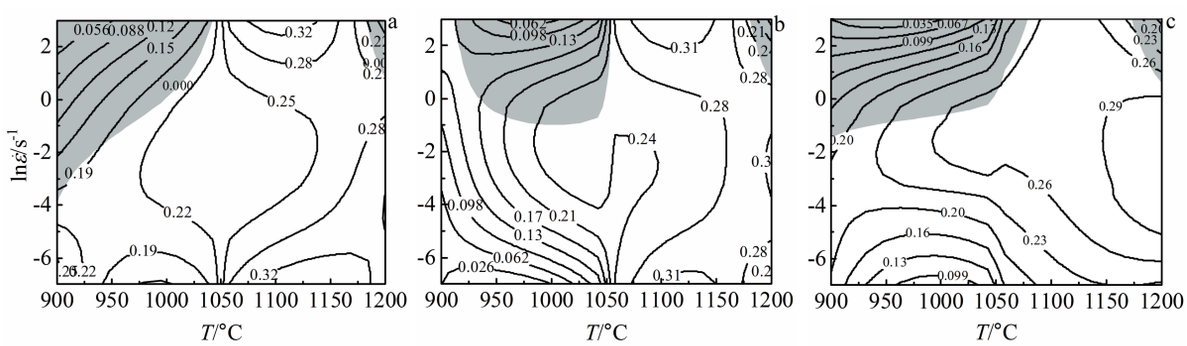

Fig.7 Heat working diagrams of Inconel 617 under the strains of 0.2 (a), 0.4 (b), and 0.6 (c)

prone to deformation and instability.

Some researchers believe that the high temperature and unstable area is a "pseudo-unstable area"[22] that has a higher concentration of recrystallization in the beginning of the deformation, and with increasing the strain, the recrystallization is completely transformed, so that the instability may be related to the multiple recrystallization of the material. In the low temperature unstable area, the temperature is low and the migration ability of the grain boundary is weak, which is not conducive to the extension of recrystallization. The second deformation time is shorter and therefore the crystallization is insufficient.

2.4 Microstructure of Inconel 617 during thermal deformation

The thermal deformation process has an important influence on the evolution of the grains. As shown in Fig. 8a, with increasing strain rate, the degree of change in the grain diameter decreases continuously. It is observed that when the strain rate is greater than 0.1 s^{-1}, the grain diameter first decreases and then increases. When the strain rate is less than 0.1 s^{-1}, the grain diameter increases. This shows that for a small strain rate, the rising temperature is conducive to the growth of dynamically recrystallized grains, while for high strain rates, as the temperature rises, the initial nucleation is slow, and is enhanced slowly. As shown in Fig. 8b, for the strain rates greater than 0.1 s^{-1}, the average aspect ratio for the deformation grain at 1100 °C is the closest to 1, and when the strain rate is less than 0.1 s^{-1}, the average aspect ratio for the deformation grain at 1000 °C is the closest to 1. This shows that the structure essentially consists of equiaxed grains at this time.

The evolution of microstructure of the Inconel 617 alloy was analyzed to verify the accuracy of the processing map, EBSD measurements were performed for the samples compressed at the same strain rate under different temperatures using the HKL-Channel 5 analysis software, and the grain size distribution results were obtained under different conditions of dynamic recrystallization, as shown in Fig.9. Under different strain rates at this temperature, the grain distribution is basically uniform, and the dynamic recrystallization process continuously occurs, which is in the safe zone of Inconel 617 alloy. It is the recrystallization diagram when the strain amount reaches the maximum under 1100 °C and different strain rates. In the diagram, different colors represent crystal grains in different states. The dynamic recrystallization grains are shown in blue, the deformed grains are shown in red, and the substructure is shown in yellow. It is observed from Fig. 9a and 9b that the dynamic recrystallization of the sample is insufficient and the sample contains a large number of deformed grains that undergo dynamic recrystallization. In contrast, Fig. 9c show that the recrystallization is sufficient and the grains are obviously refined. At the rate of 0.01 s^{-1}, many "necklace" features are observed, showing the presence of large amounts of curved grain boundaries which are typical continuous dynamic recrystallization and grain boundary reversal. This leads to increased orientation difference, resulting in the appearance of new grain and grain growth that are the features of continuous dynamic recrystallization, so it can be seen that nucleation mechanism for the Inconel 617 is comprehensive[23,24]. However, the grains are generally continuously refined with the increase in the strain rate. The degree of recrystallization first increases and then decreases with the increase in the deformation rate. This is because the low rate deformation is favorable for recrystallization due to the sufficient time for recrystallization, while when the rate reaches 1 s^{-1}, the time is not sufficient for recrystallization. The time is not sufficient because the strong nucleation mechanism cannot be promoted under high-rate deformation, leading to slow recrystallization.

Fig. 10 shows dynamic recrystallization diagrams at the temperatures of 1000, 1100, and 1200 °C at the same strain rate when the strain value reaches the maximum. When the strain rate is 0.001 s^{-1}, it can be seen that as the temperature increases, the materials are in the stable zone, dynamic recrystallization occurs, and a large number of stable substructures are produced, which also proves the accuracy of the processing map. An examination of the figures clearly shows that the crystal grains gradually increase with increasing the temperature. The recrystallized structure is also extremely sensitive to the deformation temperature, and this process is strongly related to the development of sub-grains. At 1100 °C, the deformed grains are completely replaced by recrystallized grains. At 1200 °C, the recrystallized grains rapidly grow, which may be related to the rate of grain

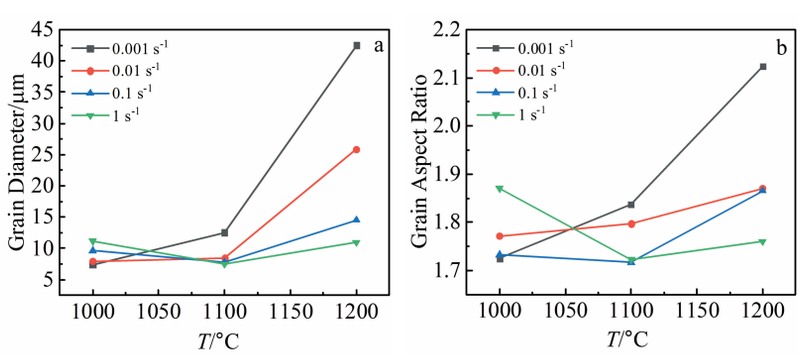

Fig.8 Average grain diameter (a) and grain aspect ratio (b) at different temperatures

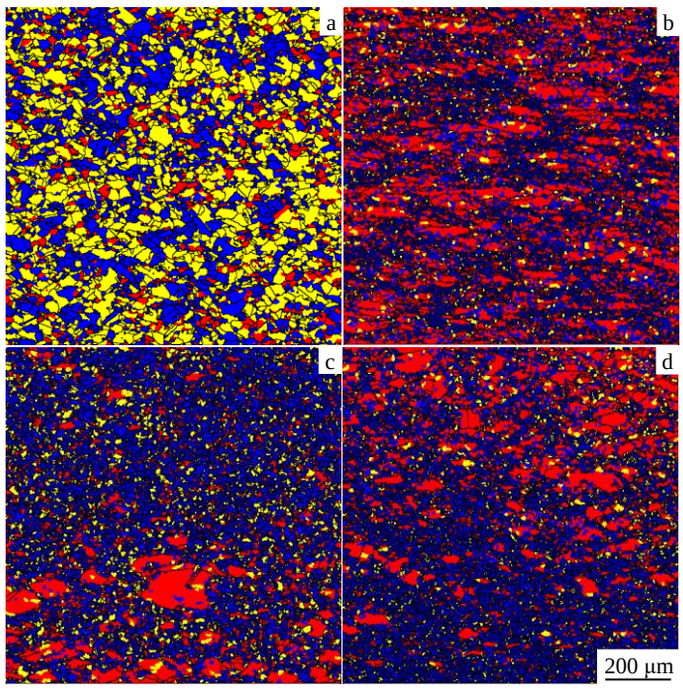

Fig.9 Dynamic recrystallization behavior of Inconel 617 alloy during hot compression at different strain rates: (a) 0.001 s^{-1}, (b) 0.01 s^{-1}, (c) 0.1 s^{-1}, and (d) 1 s^{-1}

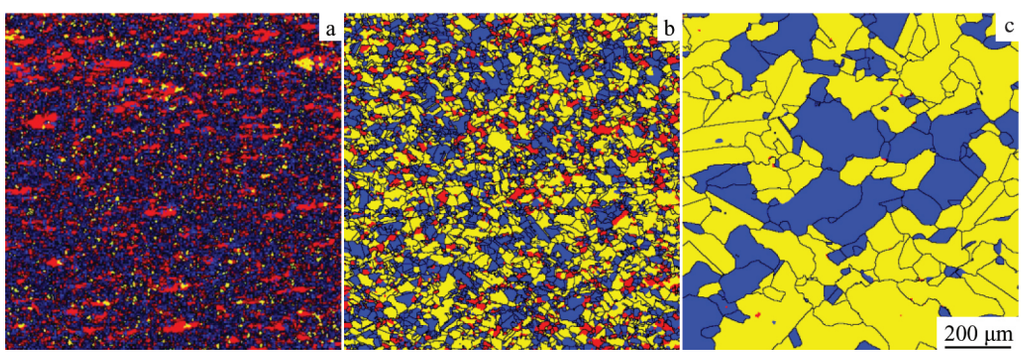

Fig.10 Dynamic recrystallization behavior of Inconel 617 alloy during hot compression at different temperatures: (a) 1000 °C, (b) 1100 °C, and (c) 1200 °C

boundary migration at high temperatures. Moreover, as the temperature increases, the mobility of the grain boundary increases, and the critical dislocation density required for the occurrence of dynamic recrystallization decreases. Recrystallization can easily occur, but with the significant increase in the substructure, the dislocation density decreases and grain growth is promoted.

3 Conclusions

1) The constitutive equation of forged Inconel 617 alloy within 900~1200 °C and 0.001~10 s^{-1} range is $\dot{\varepsilon}=2.663\ 91\times10^{18}[\sinh(0.004301944\sigma)]^{4.823\ 970\ 408}\times\exp(-502.86103/RT)$.

2) When the strain rate is high, the effect of the adiabatic temperature rise on the deformation cannot be ignored, and the maximum temperature rise can reach 70 °C. When the strain rate is lower than 0.01 s^{-1}, the system is found in the stable zone, and when the strain rate is greater than 0.01 s^{-1}, two instability zones are present in the low temperature and high speed (900~1075 °C) region and the high temperature and high speed (1175~1200 °C) region.

3) With the increase in the temperature, the grain tends to grow, which is also closely related to the increasing degree of recrystallization. However, when the strain rate is small, the grain size first decreases and then increases. The grain aspect ratio increases overall and is closest to that of equiaxed grain at 1100 °C. With the increase in the strain rate, the degree of recrystallization first increases and then decreases, and the grain size and aspect ratio roughly decrease.

References

1 Mankins W L, Hosier J C. *Metallurgical Transactions*[J], 1974, 5: 2579

2 Gosia Stein-Brzozowska, Diana M Flórez, Jörg Maier *et al. Fuel* [J], 2013, 108: 521
3 Rao C V, Srinivas N C S, Sastry G V S *et al*. *Materials Science and Engineering A*[J], 2019, 765: 138 286
4 Barbadillo J D, Baker B. *Baosteel Technical Research*[J], 2010 (S1): 84
5 Hosier J C. *Metals Engineering Quarterly*[J], 1976, 4: 51
6 Baker B A. *Hydrocarbon Engineering*[J], 2002, 7(12): 73
7 Chen Linjun. *Thesis for Master*[D]. Harbin: Harbin Institute of Technology, 2018 (in Chinese)
8 Gao Zexi. *Thesis for Master*[D]. Lanzhou: Lanzhou University of Technology, 2020 (in Chinese)
9 Cheng Jiajia. *Thesis for Master*[D]. Xi'an: Xi'an University of Technology, 2015 (in Chinese)
10 Wu J Q. *Thesis for Master*[D]. Shanghai: Shanghai Jiao Tong University, 2014 (in Chinese)
11 Han Yinben. *Thesis for Master*[D]. Shenyang: Northeastern University, 2012 (in Chinese)
12 Jia Z, Gao Z, Ji J *et al*. *Advanced Engineering Materials*[J], 2019, 21: 9
13 Zhu Lele. *Thesis for Master*[D]. Xi'an: Xi'an University of Architecture and Technology, 2015 (in Chinese)
14 Sellars C M, Mctegart W J. *Acta Metallurgica*[J], 1966, 14(9): 1136
15 Xue Cuihe. *Thesis for Master*[D]. Harbin: Harbin Institute of Technology, 2010 (in Chinese)
16 Chen Yizhe, Pang Yuhua, Wang Jianguo *et al. Rare Metal Materials and Engineering*[J], 2020, 49(9): 2956
17 Hu Chao. *Thesis for Master*[D]. Wuhan: Wuhan University of Technology, 2015 (in Chinese)
18 Wen D X, Lin Y C, Li H B *et al*. *Materials Science & Engineering A*[J], 2014, 591:183
19 Peng X, Guo H, Shi Z *et al*. *Materials Science & Engineering A* [J], 2014, 605: 80
20 Prasad Y V R K, Gegel H L, Doraivelu S M *et al*. *Metallurgical Transactions A*[J], 1984, 15(10): 1883
21 Ziegler H. *Progress in Solid Mechanics*[M]. Russia: Mir Publishing House, 1966: 91
22 Jiang He, Dong Jianxin, Zhang Maicang. *Chinese Journal of Engineering*[J], 2019, 4(41): 479 (in Chinese)
23 Jia Z, Gao Z, Ji J *et al*. *Materials*[J], 2019, 12(3): 510
24 Gao Zexi , Jia Z, Ji J *et al*. *Advanced Engineering Materials*[J], 2019, 3(22): 1 900 892

Inconel 617合金高温热变形行为与组织演变

贾　智[1,2]，俞丽丹[1]，魏保林[1]，孙　璇[1]，汪彦江[1]，刘德学[1]，丁雨田[1]
(1. 兰州理工大学 材料科学与工程学院，甘肃 兰州 730050)
(2. 兰州理工大学 有色金属先进加工与循环利用国家重点实验室，甘肃 兰州 730050)

摘　要：为解决Inconel 617合金的高温加工问题，对锻造Inconel 617合金的高温热变形行为进行了研究。利用Gleeble-3500热模拟试验机研究了Inconel 617合金在900~1200 ℃、应变速率为0.001~10 s^{-1}范围内的热塑性行为。推导了该温度和应变速率下的本构方程，得到了该温度范围内的热加工图。用电子背散射衍射研究了合金压缩后的动态再结晶。确定了失稳区的位置，并表明在热变形条件下，确实发生了动态再结晶，获得了细小的晶粒。Inconel 617热处理的最佳温度范围为1075~1175 ℃，该温度范围处于材料的安全区。

关键词：热压缩；本构方程；加工图；再结晶

作者简介：贾　智，男，1985年生，博士，副教授，兰州理工大学材料科学与工程学院，甘肃 兰州 730050，Email：jiazhi@lut.edu.cn